Available online at www.sciencedirect.com

ScienceDirect

Geochimica et Cosmochimica Acta 146 (2014) 150–163

Geochimica et Cosmochimica Acta

www.elsevier.com/locate/gca

Adsorption of radium and barium on goethite and ferrihydrite: A kinetic and surface complexation modelling study

M. Sajih [a,b], N.D. Bryan [a,c,*], F.R. Livens [a], D.J. Vaughan [b], M. Descostes [d], V. Phrommavanh [d], J. Nos [d], K. Morris [a,b]

[a] *Centre for Radiochemistry Research and Research Centre for Radwaste Disposal, The University of Manchester, Manchester M13 9PL, United Kingdom*

[b] *Research Centre for Radwaste Disposal and Williamson Research Centre for Molecular Environmental Science, The University of Manchester, Manchester M13 9PL, United Kingdom*

[c] *National Nuclear Laboratory, Chadwick House, Risley, United Kingdom*

[d] *AREVA Mines, Direction R&D, BAL 0414C, Tour AREVA, 1, Place Jean Millier, 92084 Paris La Défense Cedex, France*

Received 1 March 2014; accepted in revised form 11 October 2014; available online 18 October 2014

Abstract

Radium and barium uptake onto ferrihydrite and goethite have been studied in the concentration range 1 nM to 5 mM and from pH 4 to 10, to develop a model to predict radium behaviour in legacy uranium mining wastes. For ferrihydrite, uptake of Ra^{2+} at nM concentrations was strong at pH >7. At higher concentrations, Ba^{2+} sorption to ferrihydrite was slightly weaker than that of Ra^{2+}. Experiments with goethite showed weaker binding for both metal ions in all systems. The interactions of radium with both ferrihydrite and goethite are fully reversible. The behaviour of radium during transformation of ferrihydrite to goethite has been studied, and no evidence for irreversible incorporation within the goethite lattice was found; radium uptake to goethite was the same, whether or not it was present during its formation. Calcium competed with radium for ferrihydrite sorption only at high calcium concentrations (>10 mM). Barium is a more effective competitor, and a concentration of 1 mM reduced radium sorption. Sediment samples from a legacy uranium mining site have been analysed, and the *in situ* R_d values are consistent with radium uptake by surface coatings of ferrihydrite or goethite like phases. Surface complexation models have been developed for radium sorption to ferrihydrite and goethite which simulate the experimental data successfully. In both cases, approaches based on a single surface functional group and tetradentate binding sites simulated the data successfully. These data could be used in underpinning the safety case for legacy mining sites.
© 2014 Elsevier Ltd. All rights reserved.

1. INTRODUCTION

The interaction of metal ions with mineral surfaces is a key control on their environmental speciation and mobility. In particular, the behaviour of radionuclides in the presence of mineral surfaces is important in predicting the environmental impacts of their accidental release, or assessing the risk associated with radioactive waste disposal or with contaminated sites. The relatively large volumes of uranium mill tailings disposed near uranium mining sites contain radionuclides, including radium, which can leach out and so contaminate surface waters (Chellam and Clifford, 2002). The radium contamination associated with uranium mine wastes is significant in terms of radiological risk because of the relatively long half-life and high radiotoxicity of ^{226}Ra (Thiry and Van Hees, 2008).

* Corresponding author at: National Nuclear Laboratory, Chadwick House, Risley, WA3 6AE, United Kingdom.
E-mail address: nick.bryan@nnl.co.uk (N.D. Bryan).

http://dx.doi.org/10.1016/j.gca.2014.10.008
0016-7037/© 2014 Elsevier Ltd. All rights reserved.

Iron oxyhydroxide phases are commonly present in the environment, and have a high affinity for metal ions and radionuclides (Mishra and Tiwary, 1999). Indeed, there is evidence that they are responsible for the retention of significant amounts of radium, thus reducing its transport, even when they are present in small amounts (Nirdosh et al., 1984, 1990). In fact, iron oxides may be used as sorbents for Ra^{2+} in water treatment technologies (Chellam and Clifford, 2002). It has been suggested that the release of radium into groundwater from contaminated sites could be associated with the dissolution of iron phases, including iron oxyhydroxide coatings on other minerals (Ames et al., 1983; Gonneea et al., 2008; Thiry and Van Hees, 2008). Indeed, one study showed that radium in uranium mine wastes was associated with Fe (and Al) oxyhydroxides (Thiry and Van Hees, 2008), and iron oxides have been found to dominate radium sorption (Bassot et al., 2000a,b). Although a proportion of these Fe phases will be crystalline (e.g., goethite), some will be amorphous (Bassot et al., 2000a,b). Gonneea et al. (2008) found that sediment K_d increases with increasing Fe content, and although manganese oxides have a higher affinity for Ra^{2+}, because Fe phases are typically more abundant, they dominate radium behaviour (Gonneea et al., 2008). A number of authors have found that the interaction of Ra^{2+} with iron oxide surfaces is fast, even in natural sediment systems, and equilibrium is attained very quickly (Nirdosh et al., 1990; Gonneea et al., 2008).

The Group II elements have very similar chemistries, and there are distinct trends in their behaviours as the group is descended. For example, the magnitude of the hydration enthalpies decreases steadily from Be to Ba, as their charge densities decrease. This means that it is possible to relate the behaviour of Ra to the others in the group, and particularly barium. Mishra and Tiwary (1999) found that the sorption reactions for Group II ions are endothermic ($\Delta H(Ba) = 18.2$ kJ/mol; $\Delta H(Sr) = 21.1$ kJ/mol). They interpreted their data as evidence for Ra surface complexation, rather than ion exchange or physical sorption. Rahnemaie et al. (2006) have suggested that Mg^{2+} is mainly sorbed as a bidentate inner sphere complex, whilst Ca^{2+} forms both a bidentate inner sphere- and an outer sphere-complex with goethite. Sverjensky (2006) also predicted that the complexes of the later Group II elements are likely to be outer sphere, which is consistent with some spectroscopic data (e.g., Axe et al., 1998; Sahai et al., 2000), although not all (Collins et al., 1998). However, Sverjensky (2006) has suggested that these reported differences may be due to variations in surface properties for different samples of goethite (Sverjensky, 2005). Axe et al. (1998) found that the XAS spectra of Sr/ferrihydrite were consistent with adsorption as an outer sphere complex, rather than a surface precipitate. Hence, the studies of Sverjensky (2006) and Rahnemaie et al. (2006) suggest that Ba^{2+} and Ra^{2+} should be bound as outer sphere complexes and so barium is the most appropriate analogue for radium.

Overall, little is known about the uptake of Ra^{2+} by iron oxyhydroxide minerals. Although the stable Group II ions (Ca^{2+}; Sr^{2+}; Ba^{2+}) have been studied extensively, there are much fewer radium data available, because of its high radiotoxicity. There have been only a few studies, and those have provided limited data: for example, Ames et al. (1983) reported only 3 data points at 25 °C (all at pH 7) for ferrihydrite. Rahnemaie et al. (2006) studied the mechanism of sorption of Mg^{2+}, Ca^{2+} and Sr^{2+} on goethite, but they did not consider Ra^{2+} (or Ba^{2+}). Sverjensky (2006) reviewed and modelled a large number of Group II ion datasets for Mg^{2+}, Ca^{2+}, Sr^{2+} and Ba^{2+}, but no data were available for Ra^{2+}. Bassot et al. (2000a,b) studied radium uptake on goethite, but not ferrihydrite. Furthermore, co-precipitation and co-crystallisation of Fe phases (e.g., the conversion of ferrihydrite to goethite) will occur in the environment, and could affect radium behaviour and mobility (Thiry and Van Hees, 2008; Yee et al., 2006), although these influences are, as yet, poorly understood. Even though the crystalline forms of iron oxide are more stable than poorly ordered phases, these amorphous phases can persist in the environment and sorption processes can retard their transformation (Axe et al., 1998).

Previously, some authors have modelled Group II cation sorption to iron oxyhydroxides with simple Freundlich and Langmuir isotherms (Nirdosh et al., 1990; Mishra and Tiwary, 1999; Trivedi et al., 2001). Rahnemaie et al. (2006) found that calcium goethite sorption modelling was improved by the addition of sorbed hydrolysed calcium species ($CaOH^+$), and that the surface was indifferent to the presence of a hydroxide in the coordination sphere of the Ca. Bassot et al. (2000a,b) included the sorption of Ca and Ra hydrolysed species in their modelling of sorption on goethite. Sverjensky (2006) analysed multiple datasets for the sorption of Group II ions to oxide surfaces, including goethite, but not ferrihydrite, and suggested two general types of surface complex. The first based on a tetradentate site that can bind a Group II ion (M^{2+}) or the first hydrolysis product (MOH^+): $(\equiv SOH)_2(\equiv SO)_2M$; $(\equiv SOH)_2(\equiv SO)_2M(OH)^-$ which is more important for the larger cations (Sr^{2+} and Ba^{2+}, and by analogy Ra^{2+}). The second surface complex type is monodentate ($\equiv SO–M^+$; $\equiv SO–MOH$), which is more important for the smaller cations. For barium, only tetradentate surface species were required, albeit with two related tetradentate binary species needed to describe the data across the whole pH range: $(\equiv SOH)_2(\equiv SO)_2Ba(OH)^-$ and $(\equiv SOH)_4Ba(OH)^+$, with the second species most important in the region pH <8 (Sverjensky, 2006). Sverjensky (2006) used the same speciation code for inner and outer sphere complexes, and made no explicit changes to take account of inner versus outer sphere binding.

It is clear that there is a need to study and define Ra^{2+}/iron mineral interactions to develop a predictive capability of radium behaviour and mobility. In this work, sorption/desorption of Ra^{2+} and Ba^{2+} by goethite and ferrihydrite were studied under conditions relevant to uranium mill tailings. The reversibility of the interactions have been studied, along with the effect of mineral phase conversion and competition from Ca^{2+} and Ba^{2+}. Surface complexation modelling was applied to produce sorption constants for application in the prediction of Ra^{2+} speciation, mobility and fate. The experimental data were also assessed in the context of three environmental samples.

2. EXPERIMENTAL

All reagents used in this work were of analytical grade, and 18 MΩ water was used.

2.1. Preparation and characterisation of ferrihydrite and goethite

The iron oxyhydroxides were synthesised according to the methods described by Schwertmann and Cornel (1991). Briefly, ferrihydrite was prepared by titrating Fe(III) nitrate solution (0.2 M) with 1 M KOH solution to pH 7–8. The red brown suspension was then washed three times with deionised water to eliminate the electrolyte. Sub-samples were freeze dried for X-ray diffraction (XRD) and surface analyses. Goethite was prepared by holding freshly precipitated ferrihydrite suspension at pH 13 and 70 °C for 60 h to produce a yellow brown precipitate which was washed three times with deionised water, and then oven dried at 40 °C. The products were characterised for crystal structure, morphology and surface area, using XRD, scanning electron microscopy and BET surface area analysis. (245 ± 22 and 23.6 ± 2.0 m^2/g for ferrihydrite and goethite, respectively). Typical results obtained for ferrihydrite and goethite and analytical details are given in the supporting information, Figures S1 and S2 and Table S1.

2.2. Sorption experiments

The sorption of Ra^{2+} and Ba^{2+} on goethite and ferrihydrite was studied through batch experiments with a solid-solution ratio of 0.1 g/10 ml and 0.1 M $NaClO_4$ containing radium or barium. The pH was adjusted with 0.1 M HCl or NaOH solutions (pH 4–10) to within 0.05 pH units of the target value. The volume of acid/base added was minimised, so that the total volume added was typically <0.2 ml (2%) and always <0.5 ml (5%). Given the other experimental uncertainties, these amounts should not significantly affect the results. For goethite, 0.1 g dry solid was contacted with the $NaClO_4$ solutions to make the goethite suspensions, whereas ferrihydrite was used moist as the thick paste produced by centrifuging the washed ferrihydrite sample. The dry: wet ratios for the ferrihydrite paste were determined by oven drying at 60 °C ($n = 5$) and the appropriate mass was then added to experiments. ^{226}Ra was obtained from AEA Technology Harwell as a solution (1 MBq/ml) in 2 M HNO_3 and activity concentrations of 10, 30, 50, 70 and 100 Bq/ml ($1.2–12 \times 10^{-9}$ M; 0.271–2.71 ppb) were used in the experiments. Barium concentrations ranged between 0.001 and 5 mM (0.137–687 ppm); the Ba was added as spikes of 100 mM and 10 mM $Ba(NO_3)_2$ solutions. These concentrations for radium and barium were selected based on metal ion solubilities, environmental relevance and instrumental detection limits. All solutions were predicted to be under-saturated by thermodynamic speciation calculations performed by PHREEQC (2.18.5570) using the S.I.T. and LLNL databases. In all experiments, equilibrium was reached within 24 h contact time between solid and solution phases (supporting information, Figure S3). Prior to analysis, the solid and solution phases were separated by centrifugation (MSE Mistral 3000e centrifuge with a 43124-756 rotor, 3500 rpm, 30 min), followed by filtration (<0.22 μm PES filters). Tests confirmed that there was no measureable uptake of Ra or Ba on the filters.

Prior to the start of the experiments, PHREEQC calculations were performed (see below for details), which suggested that exposure of the experimental solutions to laboratory air would not affect the results, provided that the solution pH was less than 8. All experiments with pH >8 were performed in a controlled atmosphere glovebox (Coy Cabinet; $pCO_2 < 5$ ppm). For experiments outside of the glove box, sample tubes had a minimal headspace and were only opened for a limited time when sampling for analysis. Triplicate experiments were performed to assess the experimental error, and the pH was monitored. It was found that there was no significant difference between the radium and barium sorption experiments within and outside the glovebox, at all pH values. (supporting information, Figure S4). In experiments where Ca^{2+} or Ba^{2+} were added at high concentrations (0.001–0.5 M), work was undertaken in the CO_2 controlled glovebox to avoid over saturation of carbonate minerals.

2.3. Reversibility tests

Desorption batch experiments were carried out in triplicate for Ra^{2+} in the ferrihydrite and goethite systems in samples that had been equilibrated for 1 week prior to the desorption experiment starting. To prepare the experiment, solutions from sorption experiments that had been equilibrated for one week were carefully removed using a micro-pipette to minimise the amount of solid extracted at this stage. The tubes were then weighed in order to determine the volume of solution still in contact with solid, and so the residual Ra^{2+} activity was determined. It was found that the efficiency of solution removal was in the range 90–99%. Fresh, Ra-free solutions of the same pH and ionic strength as the sorption step were added to the Ra^{2+} labelled solid, to give the same total volume as during the sorption reaction. The systems were gently agitated and re-equilibrated for 7 days before samples were taken. In the reversibility tests, R_d values were used as a measure of binding strength, where R_d is given by,

$$R_d = \frac{\text{sorbed concentration (mol/g)}}{\text{solution concentration (mol/ml)}} \quad (1)$$

The measurements of sorbed radium concentration ($[Ra_{sorb,A}]$, mol/g) and solution radium concentration ($[Ra_{free,A}]$, mol/ml) during the adsorption step were used to correct for any solution phase radium remaining in the interstitial water during the preparation of the desorption experiment. If $[Ra_{free,D}]$ (mol/ml) is the radium concentration remaining in the solution following the desorption step, V_T (ml) is the total volume of solution used in the adsorption and desorption reactions, V_R (ml) is the volume left behind during preparation of the desorption experiment and M (g) is the mass of iron phase used in the experiment, then the desorption R_d value is given by,

$$R_{d,D} = \frac{\{([Ra_{sorb,A}] \cdot M) + ([Ra_{free,A}] \cdot V_R) - ([Ra_{free,D}] \cdot V_T)\}}{[Ra_{free,D}] \cdot M} \quad (2)$$

During the desorption step, the pH of the system was checked and controlled to within 0.05 pH units of that of the sorption experiment.

2.4. Analytical techniques

^{226}Ra concentrations were measured by gamma-ray spectrometry for radium concentrations >2 Bq/ml, using a standard geometry container and calibrating the 186.2 keV gamma line against certified, standards (AEA Technology, Harwell). The detection limit for this technique was typically 1 Bq/ml (counting efficiency of 2.5%). The detector was a Canberra high purity Ge semi-conductor detector coupled to an ORTEC 919 ADC/MCA. The counting time was variable (30 min – 2 days), depending on the sample activity: a minimum of 1000 counts were collected for each sample to reduce counting error to <3%. For lower radium activities ([^{226}Ra]<2 Bq/ml), samples were measured by a Quantulus low level liquid scintillation spectrometer using double contained samples to provide a gas tight seal which were pre-equilibrated for 28 days to ensure secular equilibrium prior to analysis. Again, sample concentrations were determined by comparison with certified standards. The counting time was variable (1 h – 3 days), depending on the sample activity: a minimum of 1000 counts were collected for each sample to reduce counting error to <3%. The detection limit for this technique was typically 0.4×10^{-3} Bq/ml (counting efficiency of ~100%). To measure Ba^{2+} concentrations, barium sample solutions (2 ml) were diluted 5-fold in 2% high purity nitric acid made from distilled HNO_3 in 18 MΩ deionised water, and analysed with a Perkin–Elmer Optima 5300 dual view ICP-AES. Sample concentrations were obtained by comparison with barium standard solutions (Alfa Aesar Specpure Multielement Plasma solution, 1000 ppm Ba) and error assessed by triplicate analyses which are included in the error bars for the barium data in the figures.

2.5. Ferrihydrite to goethite transformation experiments

Transformation of ferrihydrite to goethite was achieved following the method of Yee et al. (2006). Briefly, a ferrihydrite suspension was prepared (Schwertmann and Cornel, 1991; see above) and 500 ml of this suspension (10 g/l) was treated by bubbling O_2-free N_2 through it for one hour to remove dissolved O_2. After purging with N_2, the mineral suspension was immediately transferred into a CO_2-free, anoxic glove-box, and 10 ml aliquots of ferrihydrite suspension were placed into polypropylene tubes. Radium was added to give a concentration of 100 Bq/ml (12×10^{-9} M), and the tubes were then sealed. The samples were shaken for 24 h to ensure equilibrium prior to addition of Fe(II) solution. The ferrihydrite to goethite phase conversion was initiated by adding 1 ml Fe (II) solution into the tubes containing ferrihydrite (final [Fe(II)] = 30 mM: ferrihydrite 110 mM). Periodic sampling of $Ra^{2+}_{(aq)}$ and parallel Ra-free solids was performed over 48 h. For the experiments with radium present, the aqueous radium concentrations were measured using the procedures described above, whilst in parallel Ra-free systems, the solid phase was analysed by powder-XRD. In an additional set of experiments, radium was added after goethite formation to compare with the systems where radium was present during the conversion. At the end of crystallisation to goethite, the samples showed essentially complete conversion to goethite in 48 h by XRD, and a decrease in the surface area from 245 m^2/g to 73 m^2/g (BET).

3. RESULTS AND DISCUSSION

3.1. Ferrihydrite

Fig. 1 shows sorption isotherms (radium bound *vs* radium in solution) for sorption onto ferrihydrite at pH values of 6, 6.5 and 7 (±0.05) across the radium concentration range 1.2–12 nM (10 – 100 Bq/ml). The isotherms are all linear ($R^2 = 0.98$, 0.99 and 0.98, at pH 7, 6.5 and 6, respectively), suggesting that there was no saturation of the sorption sites, as expected given the very low concentrations of Ra in these systems. Fig. 2A shows the percentage of radium sorbed as a function of pH at three concentrations (1.2, 5.9, 12 nM). The plots show the typical sorption edges expected for the uptake of metal ions onto oxide surfaces and no significant difference between the different concentrations, again reflecting the small spread of concentrations. The radium sorption was insignificant below pH 5, and removal was quantitative (≈100%) above pH 8, with the middle of the sorption edge at pH ≈ 6.25.

The reversibility in the Ra-ferrihydrite systems was tested with desorption experiments in the pH range 6–9 ([Ra] = 12 nM). R_d values were calculated for the sorption data shown in Fig. 2A and these are plotted in Fig. 3, along with the R_d values for the equivalent desorption experiments. The data show that sorption strength increases steadily with pH, even in the pH region where the sorption data in Fig. 2A have reached a plateau, because the solution concentration continues to decrease. The data also show that the interaction between Ra^{2+} and ferrihydrite is fully reversible, since there is no significant difference between the sorption and desorption R_d values at all pH values. Benes et al. (1984) showed that radium sorption on hydrous ferric oxide was reversible at pH 6 and 7, which is consistent with this work. We have now demonstrated reversibility over a wider pH range relevant to engineered contaminated environments.

The aim of this work is to develop a model of the interaction of radium with iron oxide phases. Typically, in a surface complexation study, the sorption of the metal ion is studied over a wide range of concentrations. Due to the very high radiotoxicity of ^{226}Ra, it was not possible to perform such experiments. Also, the radium concentrations expected even at a very contaminated site will be very low (typically less than 1 nM; see below, Table 1). Therefore, experiments with Ba^{2+} as an analogue for Ra^{2+} were performed to assess heavy Group II metal ion behaviour at elevated concentrations.

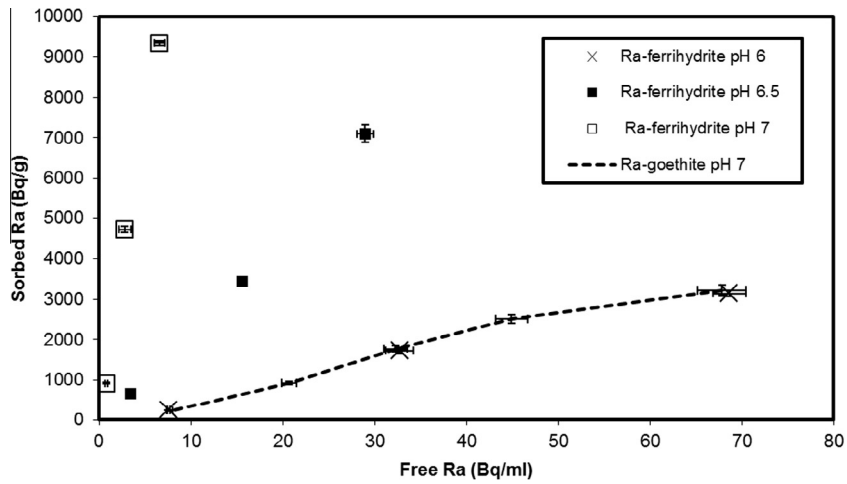

Fig. 1. Ra sorption isotherms on ferrihydrite at pH 6, 6.5 and 7 ± 0.05 pH units and goethite at pH 7 (±0.05). I = 0.1 M $NaClO_4$ and solid-solution ratio 0.1 g:10 ml. All data points are the mean of triplicate measurements $\pm 1\sigma$.

Fig. 2B shows the percentage of barium removed from solution in a ferrihydrite system versus pH for a total concentration of 36.4 μM (5 ppm). Barium shows the same general behaviour as radium. The barium data in Fig. 2B are compared with the radium data from Fig. 2A in the supporting information (Figure S5). Despite the large difference in the concentrations of barium and radium (36.4 μM and 12 nM, respectively), the behaviours are very similar, with only a small shift to higher pH (approximately 0.33 pH units) in the uptake curve. Sorption experiments were then performed in the concentration range 5–500 μM (pH = 8 ± 0.05), and the results are shown in Fig. 2C. Figure S6 shows the same data as Fig. 2C, but with a linear vertical scale. The data show that barium sorption continued across the concentration range studied.

3.2. Goethite

Fig. 1 shows a sorption isotherm for Ra on goethite determined over a radium concentration range of 1.2–12 nM. As for the ferrihydrite data (also shown in Fig. 1), the plot is linear ($R^2 = 0.97$), and as expected there was no saturation of the sorption sites by Ra^{2+}. The data show that the Ra^{2+} binding to goethite observed in these experiments is weaker than that to ferrihydrite.

Fig. 4A shows the effect of pH on radium sorption on goethite in the pH range 4–10, and for total Ra concentrations in the range 1.2–36 nM. The goethite-Ra^{2+} data show many similarities with those of ferrihydrite (Fig. 2A), although there is increased scatter in the data and a slight displacement of the sorption edge to higher pH (0.60 pH units). These goethite results are consistent with those obtained by Nirdosh et al. (1990) and Bassot et al. (2000a), who observed essentially complete removal of Ra^{2+} from solution at pH 9–10. Further, the sorption step in Fig. 4A is in the same position (pH ≈ 7) as in the data of Bassot et al. (2000a,b). The method of Nirdosh et al. (1990), had the same ionic strength as this study. Bassot et al. (2000a,b) conducted experiments at $NaClO_4$ concentrations of 0.01 and 0.1 M. Their data show only a little difference in affinity compared to our work, with a shift in the sorption edge of approximately 0.1–0.2 pH units. The R_d values for radium sorption on goethite are shown in Fig. 3. It is clear that the goethite R_d values are lower than those of ferrihydrite at any given pH, which is consistent with the shift in the sorption step to higher pH. The differences in cation binding to goethite and ferrihydrite may be rationalised in terms of the mineral structures (Charlet and Manceau, 1992; Manceau and Charlet, 1992, 1994; Manceau et al., 1992a,b; Spadini et al., 1994; Axe et al., 1998). Although goethite is more crystalline, ferrihydrite does have short range order and a layered, nano-crystalline structure. This nano-crystalline form gives ferrihydrite its very high surface area and hence its very high sorption capacities for metal ions. Desorption experiments were performed to test the reversibility of radium sorption onto goethite. As for the ferrihydrite systems, sorption was completely reversible over the range of conditions studied (Fig. 3).

Fig. 4B shows the effect of pH on the sorption of barium at a total concentration of 36 μM (5 ppm). The behaviour here was notably different to that of radium with goethite (Fig. 4A) and also barium with ferrihydrite under the same conditions (Fig. 2B), with weaker sorption. The sorption edge does not have the classical shape of the radium-goethite and barium-ferrihydrite data, and it is also displaced with its edge at pH ≈ 8.5, compared to pH ≈ 7 and pH ≈ 6.75 for radium-goethite and barium-ferrihydrite, respectively. Fig. 4C shows uptake by goethite as a function of barium concentration at pH 10 (chosen to maximise sorption), and Figure S7 shows the same data with a vertical linear scale. Although the pH in this experiment is higher, the amount of barium sorbed to the solid phase is lower than that for ferrihydrite. Comparison with other studies is difficult: we are only aware of one other report of Ba-goethite data in the literature (Hayes, 1987) which used a nitrate electrolyte background. Indeed, later analysis

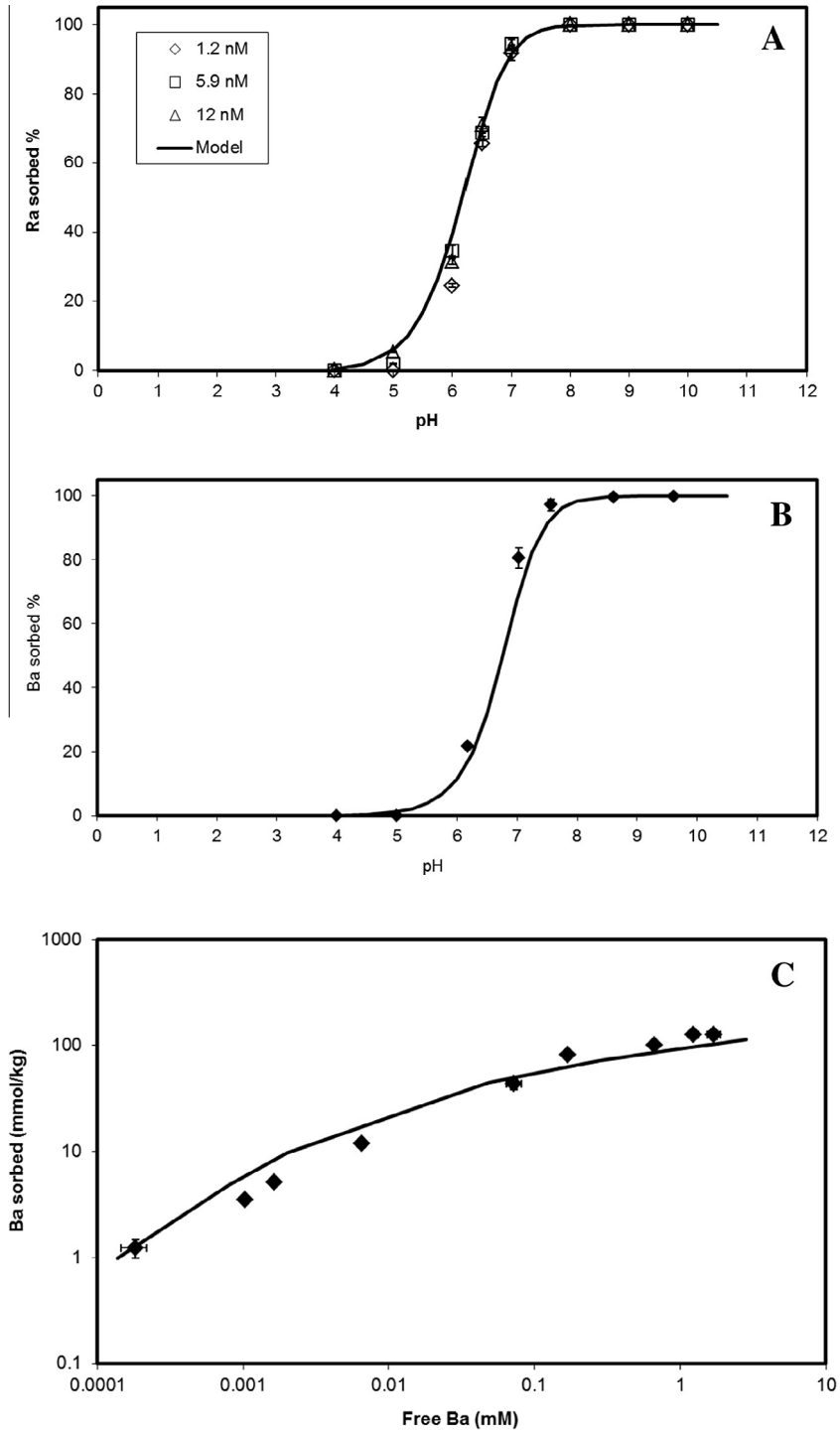

Fig. 2. Ferrihydrite data (10 g/l; I = 0.1 M): (A) pH sorption edge for Ra; (B) pH sorption edge for Ba, [Ba] = 36×10^{-6} M (5 ppm); (C) isotherm for Ba (pH = 8 ± 0.05). Symbols represent experimental data and curves represent model fits. All data points are the mean of triplicate measurements. Error bars represent $\pm 1\sigma$ derived from the triplicate measurements.

of the data showed that ternary complexes of goethite-barium-nitrate were likely to be significant (Sverjensky, 2006). The Hayes (1987) study observed a sorption step centred at a pH of approximately 7.8, with slightly different conditions compared to our work: 30 g/l; I = 0.1 M ($NaNO_3$); [Ba] = 10 μM; SA = 52 m^2/g).

3.3. Ra behaviour during transformation of ferrihydrite to goethite

Ferrihydrite is the initial product resulting from hydrolysis of an Fe(III) solution, and is a significant component of U-mining wastes. It is thermodynamically unstable

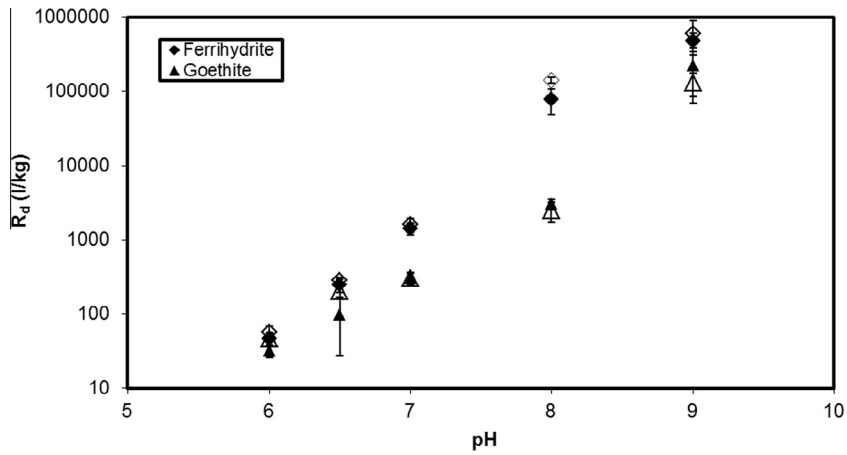

Fig. 3. Evidence of reversibility for Ra sorption/desorption on ferrihydrite and goethite at I = 0.1 M $NaClO_4$ and [Ra] = 100 Bq/ml (12 nM; 2.73 ppb), closed symbols for sorption and open symbols for desorption. Equilibration time before desorption = 1 week. All data points are the mean of triplicate measurements $\pm 2\sigma$.

and, with time, transforms to goethite or hematite or a mixture of them both, and it has been suggested that this could affect radium solubility and mobility (Thiry and Van Hees, 2008). Formation of goethite proceeds via dissolution of ferrihydrite, followed by nucleation and growth of the crystalline phase (Schwertmann and Cornel, 1991). Rapid alteration of ferrihydrite to goethite in the natural environment proceeds in the presence of Fe(II) (Yee et al., 2006), as in the synthesis method adopted in this study. The results of the transformation experiment are shown in Fig. 5. The inset shows a series of XRD peaks recorded during the conversion of ferrihydrite to goethite. At the start of the experiment, there is no (1 1 0) peak (0 h data). The peak grows over 48 h, at which time, complete conversion has been achieved. The plot in Fig. 5 shows the release of radium into solution as the conversion takes place, which is expected since goethite shows weaker sorption than ferrihydrite. Sorption decreases from nearly 100% at the start of the experiment to approximately 20% at the end of the conversion. To test the reversibility of the system, samples of converted goethite that had been formed without radium present were used in sorption experiments: the data for these experiments are plotted in Fig. 5 (single point, open symbol). Importantly, the amount of radium that is sorbed after transformation does not depend upon whether the radium was present during the transformation or whether it was added afterwards. This implies that incorporation effects are not important in these systems. The data in Fig. 5 may have implications for radium mobility, since as ferrihydrite converts to goethite at a contaminated site, an associated release of radium into solution may be expected if fresh ferrihydrite is not supplied.

3.4. Effect of Ca^{2+} and Ba^{2+} competition

Fig. 6A shows the effect of background calcium concentration on the sorption of radium onto ferrihydrite. Despite the very low concentration of radium in these experiments (12 nM; 2.71 ppb), a relatively high calcium concentration is required to produce a significant reduction in radium sorption ($[Ca^{2+}] > 0.01$ M). Hence, under many environmental conditions, calcium is not expected to affect radium behaviour significantly. Barium would typically be expected to have a lower concentration in the environment compared to calcium, because it is less abundant. However, it is a more effective competitor for radium (Fig. 6B), with inhibition of radium binding at lower concentrations (1 mM). The barium isotherm data show that at a total concentration of 1 mM, the surface loading is approximately 64% of the value at the end of the experiment in the absence of barium (Fig. 2C). The final barium concentration in Fig. 6B (10 mM) represents a total concentration greater than any of those in Fig. 2C. Hence, even at high barium loadings, a significant amount of radium is still able to sorb.

3.5. Analysis of mine site samples

Three samples of solid and *in situ* solution were obtained from a former mining site in France (Massif Central). Two mining water and sediment samples were collected prior to treatment. A third one was taken from one of the water treatment ponds at the mine. The treatment relies on the addition of NaOH to raise the pH to 9.5 to enhance the precipitation of ferrihydrite from the initially Fe rich mining waters and the subsequent sorption of ^{226}Ra. Settling and pH neutralisation takes place before release of the water to the environment. This process meets environmental requirements. Sample 1 comes from one of these treatment ponds, whilst Samples 2 and 3 were sampled from one of the naturally iron rich streams that emerge from the mine. The solid samples and the solutions were characterised by XRD for mineral structure, ESEM for morphology, ICP-AES for U and trace element concentrations, and LSC for radium concentrations (Table 1). The values of R_d are within the range of values found previously for natural

Table 1
Ra activity in solid and solution phases and R_d values for the three natural samples from the Mine site. Fe and U components are for the solid phase. Errors from Ra measurement derived from counting errors ±2σ.

Sample	Ra in solid	Ra in solution	R_d l/kg	pH	Fe weight%	U ppm	Dominant mineral phases present (determined by bulk XRD analysis)	Surface area m^2/g
1	1.41 ± 0.014 Bq/g 1.71 ± 0.02 × 10^{-13} mol/g	2.4 ± 0.056 mBq/ml 2.90 ± 0.07 × 10^{-13} mol/l	567 ± 18	7.7	1.0	65 ± 7.0	Calcite; Aragonite; Ankerite	5.44
2	38.5 ± 0.38 ppt 1.78 ± 0.016 Bq/g 2.15 ± 0.02 × 10^{-13} mol/g	0.066 ± 0.002 ppt 1.7 ± 0.045 mBq/ml 2.06 ± 0.05 × 10^{-13} mol/l	1047 ± 36	6.9	1.7	73 ± 10	Quartz; Albite; Microcline; Muscovite; Nontronite	8.99
3	48.7 ± 0.44 ppt 0.17 ± 0.005 Bq/g 2.06 ± 0.06 × 10^{-14} mol/g 4.65 ± 0.14 ppt	0.046 ± 0.001 ppt 2.1 ± 0.052 mBq/ml 2.54 ± 0.06 × 10^{-13} mol/l 0.057 ± 0.001 ppt	81 ± 4.7	6.1	1.2	15 ± 2.0	Quartz; Albite; Microcline; Muscovite; Nontronite	14.51

sediments; for example, Gonneea et al. (2008) report values in the range of 45–21,000 l/kg. The elemental concentrations present and XRD patterns of the solid samples show that the major constituents of the samples are calcite in one case, and quartz/silicates for the other two. All three samples have Fe content too low for any discrete iron-bearing phases to be detected in the XRD spectra. However, all three samples were orange/red in appearance, suggesting that the major mineral phases present were coated with iron (oxy)hydroxides. The XRD patterns for the three samples are shown in the supporting information (Figure S8), along with pictures of the samples (Figure S9) and a description of the mine site (Figures S10–S12). Figure S13 in the supporting information shows an SEM image of Sample 1 along with representative EDX spectra showing the presence of iron rich areas at the surface. R_d values for the natural samples were compared with R_d values for Ra-goethite and Ra-ferrihydrite (this study) and Ra-calcite (Jones et al., 2011), and the results are shown in Fig. 7. The natural samples gave similar R_d values to those of the iron oxides: sample 1 lies with the Ra-goethite data from this study, whilst sample 2 is definitely closer to the ferrihydrite data. Sample 3 lies in a region where there is a relatively small difference between the ferrihydrite and goethite R_d values. Hence, even though the sediments from the mine site contain Fe phases only as a minor component (as a surface coating), the interaction of radium with the surface is bracketed within the experimental R_d values for ferrihydrite and goethite, suggesting that these phases may be controlling the radionuclide behaviour at the mine site. It is well known that small amounts of Fe phases can control radium behaviour (e.g., Ames et al., 1983; Nirdosh et al., 1984, 1990; Gonneea et al., 2008; Thiry and Van Hees, 2008), and these results are consistent with that. They also suggest that sorption data for these iron phases may under certain conditions be used to predict the behaviour of the whole sediment. It is tempting to think that samples from the treatment pond behave like goethite, whilst those from before treatment behave like ferrihydrite, but more mine samples would need to be analysed to be certain.

4. SURFACE COMPLEXATION MODELLING

The diffuse double layer surface complexation approach of Dzombak and Morel (1990) was used to describe the sorption data obtained in this study for both ferrihydrite and goethite. The calculations were performed using the surface complexation modelling routine within PHREEQC, which is a geochemical speciation code. Our aim was to develop a surface complexation approach for radium that may be widely applied as part of routine speciation calculations (using PHREEQC).

The background speciation of radium ($[Ra^{2+}] = 12 \times 10^{-9}$ mol/l; 100 Bq/ml) and barium (1 μM) in solution (excluding sorption), as a function of pH and with and without equilibrium with atmospheric CO_2, was calculated. The results are given in the supporting information (Figures S14–S17) and the background thermodynamic data used in the calculations are given in Table S2. The data show that in the absence of CO_2 the 'free' $Ra^{2+}_{(aq)}$ and $Ba^{2+}_{(aq)}$ species

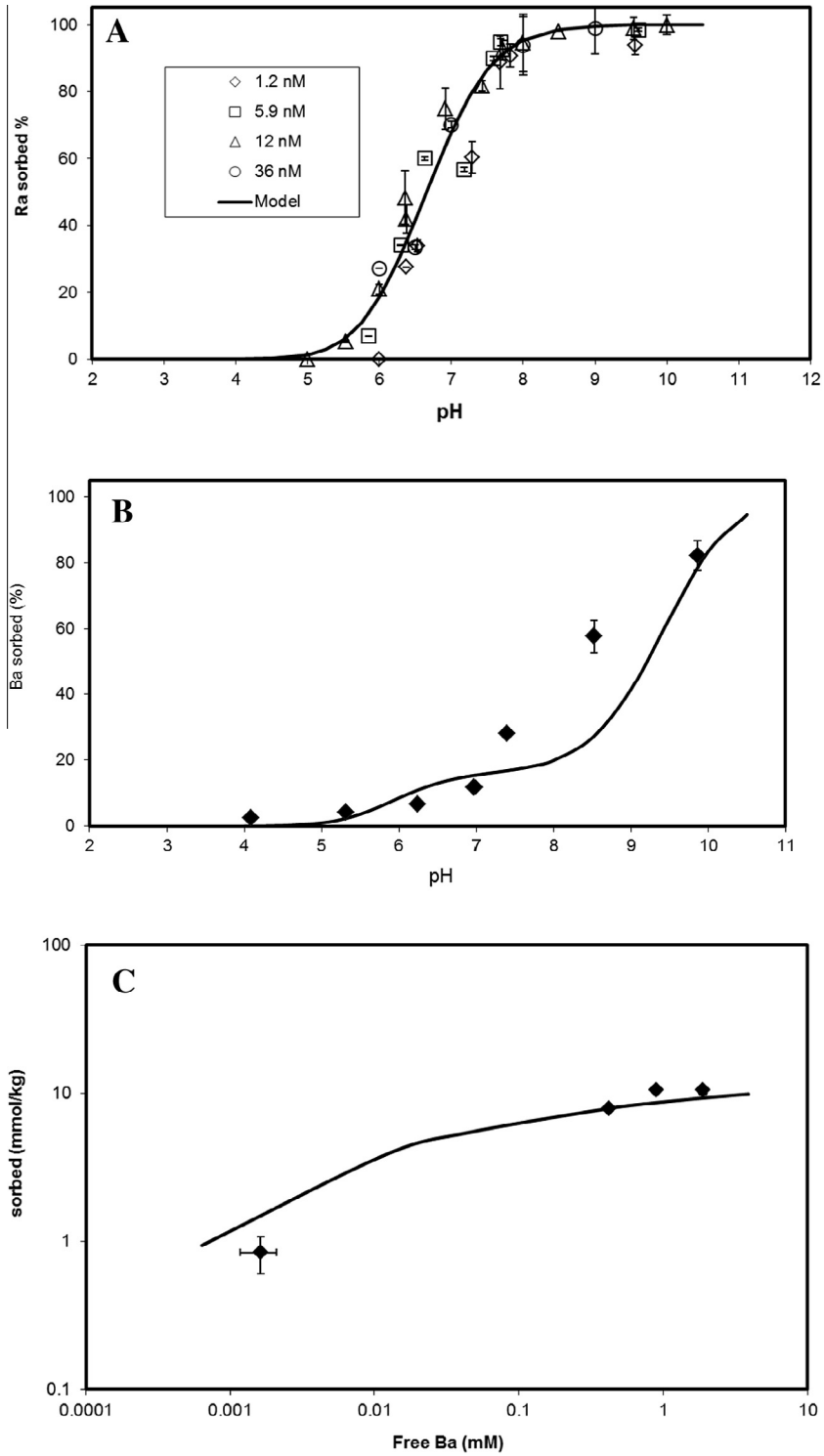

Fig. 4. Goethite sorption data (10 g/l; I = 0.1 M): (A) pH sorption edge for Ra; (B) pH sorption edge for Ba, [Ba] = 36×10^{-6} M (4.94 ppm); (C) isotherm for Ba (pH = 10 ± 0.05). Symbols represent experimental data and curves represent model fits. All data points are the mean of triplicate measurements. Error bars represent $\pm 1\sigma$ derived from the triplicate measurements.

dominate the solution speciation across the pH range, and even at pH = 10, hydroxide complexes account for less than 0.02% of the total metal concentration. In the presence of atmospheric CO_2, carbonate complexes only become significant (>1%) above pH 8.5. By this stage, the sorption is relatively strong, and this explains why experiments performed inside and outside the glovebox give similar results, even at high pH (Figure S4).

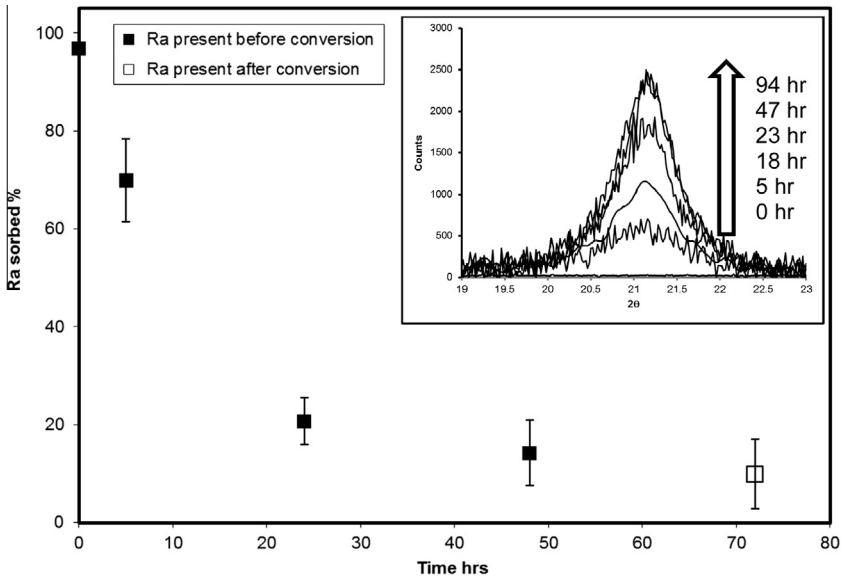

Fig. 5. Ra sorption during phase transformation from ferrihydrite to goethite over 2 days (bottom) and time-resolved XRD pattern of the (1 1 0) peak (top). Total Ra concentration = 100 Bq/ml (12 nM; 2.73 ppb) Ferrihydrite = 10 g/l; Fe(II) = 30 mM; pH 7. Errors are $\pm 2\sigma$.

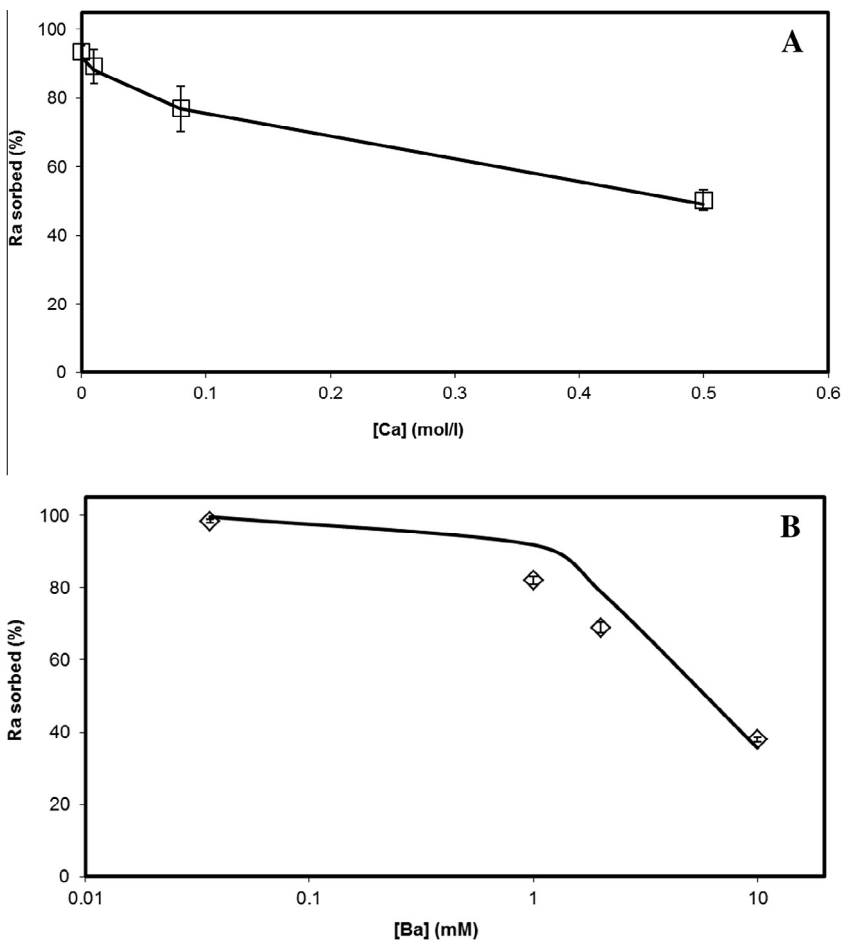

Fig. 6. Ra sorption to ferrihydrite, effect of competition (10 g/l; I = 0.1 $NaClO_4$), experimental data (symbols) and model predictions (lines): (A) effect of Ca concentration (pH = 7 ± 0.05); (B) effect of Ba concentration (pH = 8 ± 0.05). All experimental data points are the mean of triplicate measurements. Total Ra concentration = 100 Bq/ml (12 nM; 2.73 ppb). Experimental errors are $\pm 2\sigma$.

4.1. Ferrihydrite

The ferrihydrite surface complexation model described here is an adaptation of that developed for ferrihydrite (hydrous ferric oxide) by Dzombak and Morel (1990). The calculations used the experimentally determined specific surface area for ferrihydrite (245 m^2/g). The protonation constants of Dzombak and Morel (1990) were used. The protonation/deprotonation reactions and the associated equilibrium constants for the metal ion binding functional groups are:

$$\equiv\mathrm{HfoOH} + \mathrm{H}^+ \longrightarrow \equiv\mathrm{HfoOH}_2^+ \quad \log\ \mathrm{K} = 7.29 \tag{3}$$

$$\equiv\mathrm{HfoOH} \longrightarrow \equiv\mathrm{HfoO}^- + \mathrm{H}^+ \quad \log\ \mathrm{K} = -8.93 \tag{4}$$

where '≡Hfo' indicates a ferrihydrite surface species, and the equilibrium constants are those given by Dzombak and Morel (1990). For the metal ion binding sites, the tetradentate approach developed by Sverjensky (2006) was adapted. We used this method, because although it was possible to model some of the experimental data with simpler approaches, they could not model all of the systems (the fits from this approach and simpler models are discussed in Section 4.3). Sverjensky (2006) used tetradentate metal ion binding sites to model Ba^{2+} uptake to goethite. We have defined two surface reactions for Ba^{2+}:

$$4{\equiv}\mathrm{HfoOH} + \mathrm{Ba}^{2+} \rightarrow [({\equiv}\mathrm{HfoOH})_3({\equiv}\mathrm{HfoO})\mathrm{Ba}]^+ + \mathrm{H}^+ \quad \log\ \mathrm{K} = -4.45 \tag{5}$$

$$4{\equiv}\mathrm{HfoOH} + \mathrm{Ba}^{2+} + 2\mathrm{H}^+ \rightarrow [({\equiv}\mathrm{HfoOH}_2)_2({\equiv}\mathrm{HfoOH})_2\mathrm{Ba}]^{4+} \quad \log\mathrm{K} = 21.5 \tag{6}$$

and analogous reactions for Ra^{2+}:

$$4{\equiv}\mathrm{HfoOH} + \mathrm{Ra}^{2+} \rightarrow [({\equiv}\mathrm{HfoOH})_3({\equiv}\mathrm{HfoO})\mathrm{Ra}]^+ + \mathrm{H}^+ \quad \log\ \mathrm{K} = -4.45 \tag{7}$$

$$4{\equiv}\mathrm{HfoOH} + \mathrm{Ra}^{2+} + 2\mathrm{H}^+ \rightarrow [({\equiv}\mathrm{HfoOH}_2)_2({\equiv}\mathrm{HfoOH})_2\mathrm{Ra}]^{4+} \quad \log\mathrm{K} = 22.2 \tag{8}$$

In order to fit the data, the surface complexes needed to be slightly different to those of Sverjensky, who defined $(\equiv\mathrm{SOH})_2(\equiv\mathrm{SO})_2\mathrm{Ba(OH)}^-$ and $(\equiv\mathrm{SOH})_4\mathrm{Ba(OH)}^+$: this is probably due to the fact that the solid phase here is different, ferrihydrite instead of goethite.

To model the effect of Ca^{2+} competition, we used the complexes and equations used by Sverjensky (2006) for sorption of Ca^{2+} to goethite, although the equilibrium constants had to be adapted to obtain the best fit for ferrihydrite:

$$4{\equiv}\mathrm{HfoOH} + \mathrm{Ca}^{2+} \rightarrow [({\equiv}\mathrm{HfoOH})_2({\equiv}\mathrm{HfoO})_2\mathrm{Ca}] + 2\mathrm{H}^+ \quad \log\ \mathrm{K} = -9.0 \tag{9}$$

$$4{\equiv}\mathrm{HfoOH} + \mathrm{Ca}^{2+} + \mathrm{H_2O} \rightarrow [({\equiv}\mathrm{HfoOH})_2({\equiv}\mathrm{HfoO})_2\mathrm{Ca(OH)}]^- + 3\mathrm{H}^+ \quad \log\mathrm{K} = -16.0 \tag{10}$$

$$\equiv\mathrm{HfoOH} + \mathrm{Ca}^{2+} + \mathrm{H_2O} \rightarrow [({\equiv}\mathrm{HfoO})\mathrm{Ca(OH)}] + 2\mathrm{H}^+ \quad \log\ \mathrm{K} = -12.4 \tag{11}$$

The values of the equilibrium constants and the total surface functional group concentration (1.75×10^{-3} mol/g) were obtained by fitting of the experimental data. Speciation diagrams showing the distribution of radium and barium between the solution and the two model sites are given in Figures S18 and S19.

4.2. Goethite

The goethite surface complexation model was based on that of Sverjensky (2006), and uses a single surface functional group (≡GoeOH). The calculations used the experimentally determined specific surface area (23.6 m^2/g). The protonation/deprotonation reactions and equilibrium constants are:

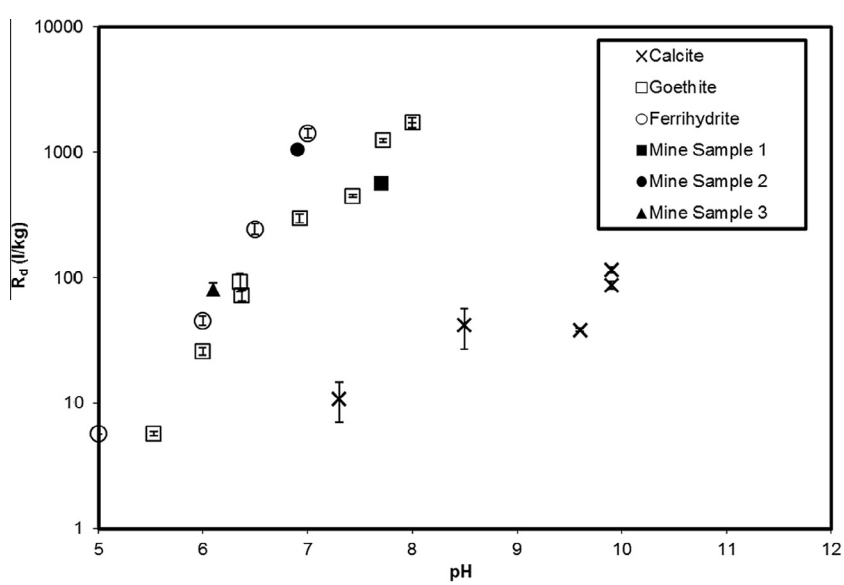

Fig. 7. R_d values as a function of pH for Ra sorption on goethite and ferrihydrite (this study), mine site samples, and calcite (Jones et al., 2011). All data points are the mean of triplicate measurements $\pm 1\sigma$, except natural samples are $\pm 2\sigma$.

$$\equiv\text{GoeOH} + \text{H}^+ \rightarrow \equiv\text{GoeOH}_2^+ \quad \log\ \text{K} = 4.8 \tag{12}$$

$$\equiv\text{GoeOH} \rightarrow \equiv\text{GoeO}^- + \text{H}^+ \quad \log\ \text{K} = -10.4 \tag{13}$$

where '≡Goe' indicates a goethite surface complex. These are the reactions and constants used by Sverjensky (2006). The total surface site concentration was $[\equiv\text{GoeOH}]_{\text{Total}} = 6.4 \times 10^{-5}$ mol/g), which was determined by fitting of the data. The reactions and constants for the sorption of Ba^{2+} were:

$$4\equiv\text{GoeOH} + \text{Ba}^{2+} \rightarrow [(\equiv\text{GoeO})(\equiv\text{GoeOH})_3\text{Ba}]^+ + \text{H}^+ \quad \log\ \text{K} = -4.9 \tag{14}$$

$$4\equiv\text{GoeOH} + \text{Ba}^{2+} \rightarrow [(\equiv\text{GoeOH})_4\text{Ba}]^{2+} \quad \log\ \text{K} = 3.8 \tag{15}$$

Analogous reactions were defined for Ra^{2+}:

$$4\equiv\text{GoeOH} + \text{Ra}^{2+} \rightarrow [(\equiv\text{GoeO})(\equiv\text{GoeOH})_3\text{Ra}]^+ + \text{H}^+ \quad \log\ \text{K} = -2.5 \tag{16}$$

$$4\equiv\text{GoeOH} + \text{Ra}^{2+} \rightarrow [(\equiv\text{GoeOH})_4\text{Ra}]^{2+} \quad \log\ \text{K} = 3.85 \tag{17}$$

The surface complexes are different to those used by Sverjensky (2006), who used $(\equiv\text{SOH})_2(\equiv\text{SO})_2\text{Ba(OH)}^-$ and $(\equiv\text{SOH})_4\text{Ba(OH)}^+$. However, in surface complexation modelling, it is not possible to distinguish between ternary complexes with a hydroxide ion and a binary complex with one more surface functional group deprotonated. i.e., the same fit could have been obtained using $[(\equiv\text{GoeOH})_4\text{Ra(OH)}]^+$ instead of $[(\equiv\text{GoeO})(\equiv\text{GoeOH})_3\text{Ra}]^+$ and so mathematically, one of our species is equivalent to one of Sverjensky's. We used surface complexes without bound hydroxide ions, because the solution speciation calculations show that hydroxide complexes are not predicted to be important in solution in the pH range that we have studied (Figures S14 and S16, supporting information), and so it seems unlikely that they will be preferred on the surface. The fact that we have used a pair of complexes with on overall higher degree of protonation than those of Sverjensky (2006) is due to the fact that we have recorded Ba sorption starting at pH 4, whilst the data of Hayes (1987) modelled by Sverjensky (2006) start at pH = 6. The difference may be due to the different conditions in the two studies, and in particular the different electrolytes, since the nitrate electrolyte used by Hayes (1987) may have formed ternary complexes (Sverjensky, 2006). Speciation diagrams showing the distribution of radium and barium between the solution and the two model sites are given in Figures S20 and S21.

4.3. Data fitting

The fits obtained to the simple sorption data with the ferrihydrite model are shown in Figs. 2(A–C). The Ba data were fitted first to define the reactions and the total functional group concentration. The fits to both the sorption of radium and barium versus pH and the barium concentration isotherm are good. The relative magnitude of the radium and barium equilibrium constants are consistent with the slightly stronger binding of radium observed in Fig. 2A compared to that of barium in Fig. 2B. Sverjensky (2006) predicted that radium binding should be lower than that of barium. However, the radium data in Fig. 2A are at a much lower concentration (12 nM) than the barium data in Fig. 2B (36 μM), and it is possible that the slightly higher binding strength results from the concentration difference, perhaps due to a small concentration of slightly higher affinity sites that are only evident at lower metal concentrations.

The model fit to the calcium competition data is shown in Fig. 6A. The fit to the experimental data is excellent, but this is not surprising given that the calcium equilibrium constant values were chosen in order to fit these data. Note, the reactions and equilibrium constants defined above for Ca^{2+} are empirical and suitable only for taking into account the effect of calcium competition on radium sorption: they should not be used for predicting calcium sorption.

The fit to the barium competition data is more impressive as the data in Fig. 2 were used to define the model parameters which were then applied 'blind' to generate the data in Fig. 6B which is within ca 10% of the correct values.

The goethite systems were much harder to fit than those with ferrihydrite (Fig. 4). As for the ferrihydrite system, the barium data (Fig. 4B and C) were fitted first followed by the radium system (Fig. 4A). Although the radium data show a normal pH sorption step, the goethite behaviour shows a different shape. Barium binding by goethite has been measured previously by Hayes (1987). When Sverjensky (2006) modelled the data of Hayes, he had to include nitrate ternary complexes to explain the sorption data, because the sorption could not be modelled with simple, binary surface complexes. This could be justified, because solution phase nitrate complexes of Ba^{2+} are known. In this case, the background electrolyte anion is perchlorate, which was chosen as a non-complexing electrolyte, and so perchlorate ternary complexes were not included here. The fit is less good this time: the model fit misses one of the data points in Fig. 4C, and although the model predicts that sorption should increase over the pH range 5–10, it does not match the shape of the experimental data (Fig. 4B). The fit to the radium data is much closer (Fig. 4A).

Previous authors have used a variety of approaches to model the uptake of Group II metal ions by ferric oxides (see above): some have used simpler, single monodentate binding equations (e.g., Mishra and Tiwary, 1999), whilst others have defined multiple binding equations (e.g., Bassot et al., 2000a,b) and multidentate binding sites (Sverjensky, 2006). In many cases, it is possible to model experimental data successfully with more than one approach, because all surface complexation modelling is to some extent semi-empirical. Appendix E in the supporting information shows examples of the fits obtained with simpler models. The only previous surface complexation modelling study for radium is that of Bassot et al. (2000a,b) for goethite sorption. They used two monodentate reactions, but they did not model barium simultaneously, and so all of their data are at trace radium concentrations. It would be possible to simulate the

radium/goethite data from this study with such an approach (supporting information, Appendix E).

In particular, the surface complexation model described by Dzombak and Morel (1990) has been used widely for the sorption of a number of metal ions by ferrihydrite (hydrous ferric oxide). Therefore, Appendix E (supporting information) contains a fit to the ferrihydrite data using the surface site types, densities, pK_a values and specific surface area exactly as used by Dzombak and Morel (1990). The equations in Appendix E would allow radium predictions to be made using existing Dzombak and Morel (1990) type models.

The modelling results are consistent with a similar complexation mechanism for both barium and radium, since the same equations could be used to simulate the behaviour of the two metals in the ferrihydrite and goethite systems. For the surface complexation calculations described here, it was found that the inclusion of atmospheric CO_2 made no significant difference to the results. The simulations predict that the presence of CO_2 does not have an effect on sorption at pH >8, as barium and radium bind to the mineral surface rather than forming complexes with carbonate in solution.

The aim of this study is to provide a surface complexation model suitable for predicting radium sorption at contaminated sites. Experiments with radium were only possible up to a concentration of 12 nM (2.71 ppb), with data at higher concentrations provided by using barium as an analogue. For both ferrihydrite and goethite, there are slightly different equilibrium constants; those for goethite being lower. In a radiological safety case, calculations should be conservative, i.e., they should not overestimate sorption. For systems where the radium concentrations are of the order of nanomolar or less, then the radium constants defined above are the most appropriate to use. However, if the total radium concentrations are higher, the barium values may be more appropriate, because they will always predict a higher concentration in solution. The radium concentrations in the waters taken from the mine sites studied here (and indeed within any typical contaminated site) are very low ($2–3 \times 10^{-13}$ mol/l), and so the radium constants are appropriate. Moreover, such an approach could be applied to classical mining water treatment processes using Ba- to coprecipitate ^{226}Ra in barite, especially in the case of Fe rich mining waters.

5. CONCLUSIONS

As expected, radium sorption to both ferrihydrite and goethite is linear up to radium concentrations of 12 nM (2.71 ppb). For ferrihydrite and radium, a typical sorption step is observed, centred at pH ≈ 6.25. The barium step is slightly displaced by approximately 0.3 pH units, indicating slightly weaker sorption. The radium interaction with ferrihydrite becomes stronger with increasing pH, with R_d increasing from 45 to 470,000 l/kg across the pH range 6–9. Radium uptake by goethite is slightly weaker; R_d increases from 32 to 220,000 l/kg across the same pH range, and the sorption step is at pH ≈ 7. For both ferrihydrite and goethite in a 0.1 M $NaClO_4$ background electrolyte system, the interaction with Ra^{2+} is completely reversible, so that thermodynamic modelling approaches (such as surface complexation modelling) are suitable for predicting the effect of sorption to these phases and Ra^{2+} mobility in the environment. Further, there is no evidence for incorporation of radium within goethite during phase transformation from ferrihydrite to goethite. Hence, a coupled chemical transport model that contains routines to account for sorption to ferrihydrite and goethite should be able to simulate radium behaviour, even where mineral phase transformations are taking place due to, for example, bioreduction processes (e.g., Thorpe et al., 2012). Calcium has been found to compete with radium for sorption to ferrihydrite, but the effect is only significant at high concentrations ([Ca] > 0.01 M at pH 7). Although barium is able to suppress radium sorption at lower concentrations (1 mM), it will have lower concentrations in the environment, and so in most cases, competition will not be significant.

It has been established previously that sorption of radium in the environment is expected to be dominated by iron phases (e.g., Ames et al., 1983; Gonneea et al., 2008) and here analysis of the samples from a legacy uranium mining site has shown that uptake onto the *in situ* sediments is consistent with this model: The R_d values determined here for ferrihydrite and goethite do predict the solid: solution partition for the mine site samples. This is despite the fact that the mine site samples are predominantly calcite, quartz and silicate phases, and so it seems that radium behaviour at the site may be controlled by small amounts of ferrihydrite-like and goethite-like phases that are coating the bulk minerals.

Surface complexation models have been developed to simulate the interactions of Ra^{2+} and Ba^{2+} with ferrihydrite and goethite. For both phases, two equations have been defined for each ion with each surface type. All of the surface species are tetradentate in terms of a single surface functional group. For each surface, surface complexes with the same stoichiometry are able to simulate both radium and barium behaviour. However, different complexes are required for each phase: $[(\equiv HfoOH)_3(\equiv HfoO)M]^+$ and $[(\equiv HfoOH_2)_2(\equiv HfoOH)_2M]^{4+}$ for ferrihydrite; $[(\equiv GoeO)(\equiv GoeOH)_3M]^+$ and $[(\equiv GoeOH)_4M]^{2+}$ for goethite. Higher equilibrium constants are required for radium binding for both phases. This may be due to the large differences in concentration between the radium and barium data, or it could be due to a small intrinsic difference between the Ra^{2+} and Ba^{2+} interactions. Given that the interaction of radium with both phases is reversible and sorption is unaffected by phase transformations, a surface complexation approach should be able to predict radium solubility and mobility in the environment where these two phases dominate the iron mineralogy.

In this work, it was found that the tetradentate model of Sverjensky provided the best fit to the experimental data. However, the ferrihydrite (hydrous ferric oxide) surface complexation model of Dzombak and Morel (1990) is very widely applied and complexation constants exist for a wide range of metal ions. Therefore, Appendix E contains the best possible fit to the ferrihydrite data using this approach, so that constants are available for this model too.

ACKNOWLEDGMENTS

The authors acknowledge AREVA Mining and NERC grant NE/F017979/1 for supporting this work and Paul Lythgoe (The University of Manchester) for elemental analysis. They also thank associate editor Annie Kersting and three anonymous reviewers for their comments.

APPENDIX A. SUPPLEMENTARY DATA

Supplementary data associated with this article can be found, in the online version, at http://dx.doi.org/10.1016/j.gca.2014.10.008.

REFERENCES

Ames L. L., McGarrah J. E., Walker B. A. and Salter P. F. (1983) Uranium and radium sorption on amorphous ferric oxyhydroxide. *Chem. Geol.* **40**, 135–148.

Axe L., Bunker G. B., Anderson P. R. and Tyson T. A. (1998) An XAFS analysis of strontium at the hydrous ferric oxide surface. *J. Colloid Interface Sci.* **199**, 44–52.

Bassot S., Stammose D., Mallet C., Ferreux J. M. and Lefebvre C. (2000a) Study of the radium sorption/desorption on goethite. *Proceedings of the 10th International Congress of the International Radiation Protection Association*. http://www.irpa.net/irpa10/topic.html.

Bassot S., Malle C. and Stammose D. (2000b) Experimental study and modeling of the radium sorption onto goethite. *MRS Proc.* **663**, 1081.

Benes P., Strejc P. and Lukavec Z. (1984) Interaction of radium with freshwater sediments and their mineral components. I. Ferric hydroxide and quartz. *J. Radioanal. Nucl. Ch.* **82**, 275–285.

Charlet L. and Manceau A. A. (1992) X-ray absorption spectroscopic study of the sorption of Cr(III) at the oxide-water interface. II. Adsorption, coprecipitation, and surface precipitation on hydrous ferric oxide. *J. Colloid Interface Sci.* **148**, 443–458.

Chellam S. and Clifford D. A. (2002) Physical–chemical treatment of groundwater contaminated by leachate from surface disposal of uranium tailings. *J. Environ. Eng-ASCE.* **128**, 942–952.

Collins C. R., Sherman D. M. and Valva Ragnarsdottir K. V. (1998) The adsorption mechanism of Sr^{2+} on the surface of goethite. *Radiochim. Acta* **81**, 201–206.

Dzombak D. A. and Morel M. M. F. (1990) *Surface Complexation Modeling: Hydrous Ferric Oxide*. Wiley-Interscience, New York.

Gonneea M. E., Morris p. J., Dulaiova H. and Charette M. A. (2008) New perspectives on radium behavior within a subterranean estuary. *Mar. Chem.* **109**, 250–267.

Hayes K. F. (1987) Equilibrium, spectroscopic, and kinetic studies of ion adsorption at the oxide/aqueous interface. Ph. D. thesis, Stanford Univ, USA.

Jones M. J., Butchins L. J., Charnock J. M., Pattrick R. A. D., Small J. S., Vaughan D. J., Wincott P. L. and Livens F. R. (2011) Reactions of radium and barium with the surfaces of carbonate minerals. *Appl. Geochem.* **26**, 1231–1238.

Manceau A. and Charlet L. (1992) X-ray absorption spectroscopic study of the sorption of Cr(III) at the oxide-water interface. I. Molecular mechanism of Cr(III) oxidation on Mn oxides. *J. Colloid Interface Sci.* **148**, 425–442.

Manceau A. and Charlet L. (1994) The mechanism of selenate adsorption on goethite and hydrous ferric oxide. *J. Colloid Interface Sci.* **168**, 87–93.

Manceau A., Gorshkov A. I. and Drits V. A. (1992a) Structural chemistry of Mn, Fe Co, and Ni in manganese hydrous oxides: Part I. Information from XANES spectroscopy. *Am. Mineral.* **77**, 1133–1143.

Manceau A., Gorshkov A. I. and Drits V. A. (1992b) Structural chemistry of Mn, Fe Co, and Ni in manganese hydrous oxides: Part II. Information from EXAFS spectroscopy and electron and X-ray diffraction. *Am. Mineral.* **77**, 1144–1157.

Mishra S. P. and Tiwary D. (1999) Ion exchangers in radioactive waste management. Part XI. Removal of barium and strontium ions from aqueous solutions by hydrous ferric oxide. *Appl. Radiat. Isot.* **51**, 359–366.

Nirdosh I., Muthuswami S. V. and Baird M. H. I. (1984) Radium in uranium mill tailings – Some observations on retention and removal. *Hydrometallurgy* **12**, 151–176.

Nirdosh I., Trembley W. B. and Johnson C. R. (1990) Adsorption–desorption studies on the ^{226}Ra-hydrated metal oxide systems. *Hydrometallurgy* **24**, 237–248.

Rahnemaie R., Hiemstra T. and van Riemsdijk W. H. (2006) Inner- and outer-sphere complexation of ions at the goethite-solution interface. *J. Colloid Interface Sci.* **297**, 379–388.

Sahai N., Carroll S. A., Roberts S. and O'Day P. A. (2000) X-ray absorption spectroscopy of strontium(II) coordination. II. Sorption and precipitation at kaolinite, amorphous silica, and goethite surfaces. *J. Colloid Interface Sci.* **222**, 198–212.

Schwertmann U. and Cornel R. M. (1991) *Iron Oxides in the Laboratory, Preparation and Characterization*. VCH, Weinheim.

Spadini L., Manceau A., Schindler P. W. and Charlet L. (1994) Structure and stability of Cd^{2+} surface complexes on ferric oxides.1.Results from EXAFS spectroscopy. *J. Colloid Interface Sci.* **168**, 73–86.

Sverjensky D. A. (2005) Prediction of surface charge on oxides in salt solutions: Revisions for 1:1 (M+L-) electrolytes. *Geochim. Cosmochim. Acta* **69**, 225–257.

Sverjensky D. A. (2006) Prediction of the speciation of alkaline earths adsorbed on mineral surfaces in salt solutions. *Geochim. Cosmochim. Acta* **70**, 2427–2453.

Thiry Y. and Van Hees M. (2008) Evolution of pH, organic matter and ^{226}radium/calcium partitioning in U-mining debris following revegetation with pine trees. *Sci. Total Environ.* **393**, 111–117.

Thorpe C. L., Law G. T. W., Boothman C., Lloyd J. R., Burke I. T. and Morris K. (2012) The synergistic effects of high nitrate concentrations on sediment bioreduction. *Geomicrobiol. J.* **29**, 484–493.

Trivedi P., Axe L. and Dyer J. (2001) Adsorption of metal ions onto goethite: Single-adsorbate and competitive systems. *Colloid Surf., A* **191**, 107–121.

Yee N., Shaw S., Benning L. G. and Nguyen T. H. (2006) The rate of ferrihydrite transformation to goethite via the Fe(II) pathway. *Am. Mineral.* **91**, 92–96.

Associate editor: Annie B. Kersting